General Disclaimer

One or more of the Following Statements may affect this Document

- This document has been reproduced from the best copy furnished by the organizational source. It is being released in the interest of making available as much information as possible.

- This document may contain data, which exceeds the sheet parameters. It was furnished in this condition by the organizational source and is the best copy available.

- This document may contain tone-on-tone or color graphs, charts and/or pictures, which have been reproduced in black and white.

- This document is paginated as submitted by the original source.

- Portions of this document are not fully legible due to the historical nature of some of the material. However, it is the best reproduction available from the original submission.

INVERSE TRANSONIC AIRFOIL DESIGN METHODS

INCLUDING BOUNDARY LAYER AND VISCOUS INTERACTION EFFECTS

AEROSPACE ENGINEERING DEPARTMENT

TEXAS A&M UNIVERSITY

SEMIANNUAL PROGRESS REPORT

AUGUST 1, 1981 - JANUARY 31, 1982

TAMRF REPORT NO. 3224-82-01
FEBRUARY 1982

LELAND A. CARLSON
ASSISTANT DEAN AND
PROFESSOR OF AEROSPACE ENGINEERING
TEXAS A&M UNIVERSITY
COLLEGE STATION, TX 77843

TEXAS ENGINEERING EXPERIMENT STATION

INVERSE TRANSONIC AIRFOIL DESIGN METHODS INCLUDING BOUNDARY LAYER AND VISCOUS INTERACTION EFFECTS

Semiannual Progress Report

August 1, 1981 - January 31, 1982

TAMRF Report No. 3224-82-01

February 1982

Leland A. Carlson
Assistant Dean and
Professor of Aerospace Engineering
Texas A&M University
College Station, TX 77843

The NASA Technical Officer for Grant NSG-1174 is Mr. Joel Everhart, Subsonic-Transonic Aerodynamics Division, NASA Langley.

INVERSE TRANSONIC AIRFOIL DESIGN METHODS
INCLUDING BOUNDARY LAYER AND VISCOUS INTERACTION EFFECTS

I. Introduction

This report covers the period 1 August 1981 to 31 January 1982. The primary task during this reporting period was the extension of the grid embedment technique for TRANDES to transonic cases with viscous interaction. In addition, the study of the massive separation model (SKANFP) to medium speed cases was continued.

II. Personnel

The staff assigned to the project during this reporting period were:

Leland A. Carlson, Principal Investigator

August -- Approximately ½ time

Sept.-Nov. -- Approximately 1/8 time

Dec. -- Approximately 1/4 time

Christopher Reed, Graduate Research Assistant

August - December -- ½ time

The work assignments during this reporting period were:

(a) Grid Embedment (Carlson and Reed)

(b) Massive Separated Flow (Carlson)

III. Embedded Grid Studies

In the last progress report[1], the second phase of the embedded grid studies was discussed. In that phase, the embedded grid scheme was redone to include upwind differencing and, as necessary, time-like damping.

It utilized a body fitted orthogonal curvilinear coordinate system, as shown on Figure 1, embedded in the overall cartesian system; and the appropriate full inviscid potential flow equation was solved using SLOR sweeping from F to B and F to C respectively. The size and discretization of this embedded grid is variable and determined by user selected input variables. This technique has been successfully applied to incompressible, slightly supercritical, and supercritical cases. However, in its second phase form, this approach did not include the effects of weak viscous interaction.

During the present reporting period, this embedded scheme has been extended to include the effects of laminar-turbulent viscous interaction. As before, this new code uses for the embedded grid an orthogonal body-fitted coordinate system in which one grid line coincides with the surface of the airfoil. At this grid line, the no normal flow boundary condition is enforced in the inviscid case. In the viscous case, an appropriate tangency boundary condition is imposed at the location of the displacement surface.

The boundary condition imposed on the outer boundary of the embedded grid requires that the embedded grid solution interface smoothly with the main grid solution. An initial embedded grid solution based upon the main grid solution is also needed to start the embedded iterative scheme. In order to satisfy these two conditions, a linear interpolation is used to obtain a perturbation potential ϕ value at each embedded grid point from the main grid ϕ values. The ϕ values around the outer embedded grid are then held constant during the embedded relaxation process to satisfy the outer boundary condition.

The incorporation of weak viscous effects into the analysis of the airfoil flowfield is accomplished in the current program by assuming that the inviscid streamlines follow a displacement surface having ordinates and slopes different from the actual airfoil.

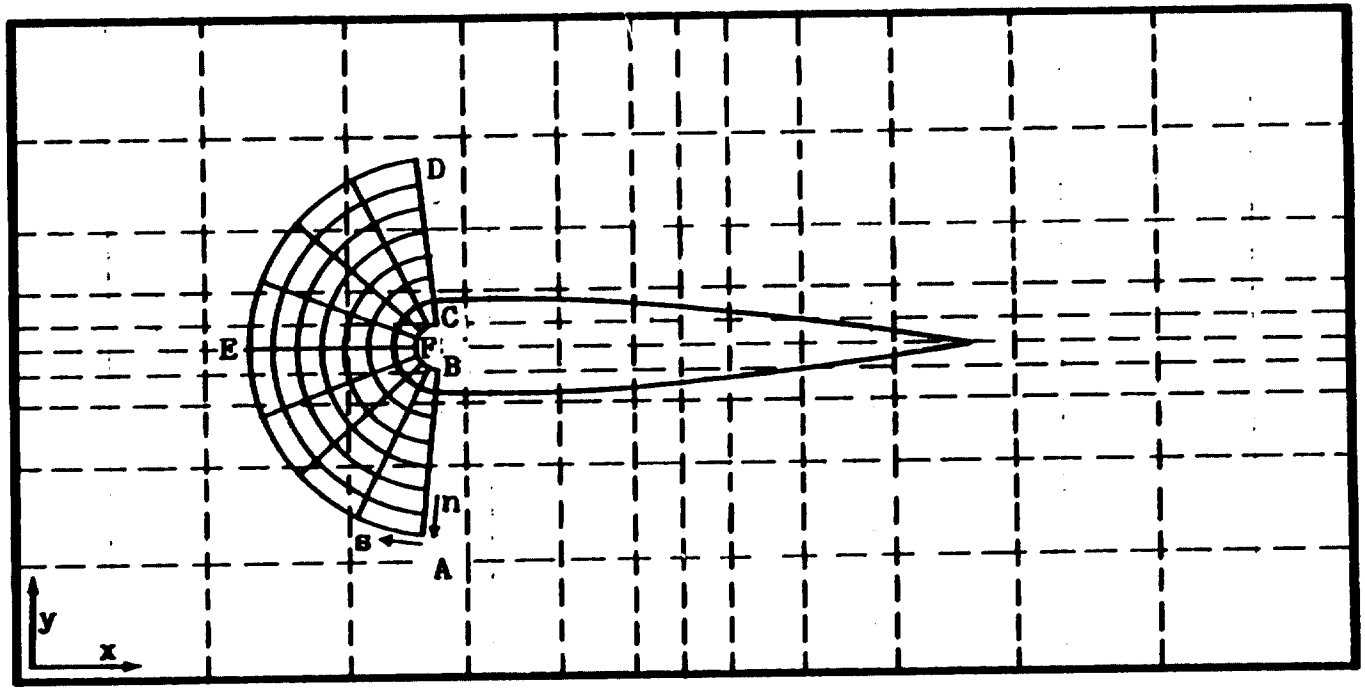

Figure 1 - Computational Grid System used in TRANDES

The flowfield is then solved inviscidly around this displacement surface to obtain the pressure distribution around the airfoil.

The ordinates of the displacement surface are obtained by adding a calculated boundary layer displacement thickness to the airfoil ordinates. In order to calculate the boundary layer displacement thickness (δ^*) the pressure distribution around the airfoil must be known. Therefore, an initial inviscid flowfield solution must be obtained before viscous interaction can be introduced. Once viscous interaction has been introduced, the flowfield must be solved iteratively along with the boundary layer in order to obtain the steady state solution. The values of displacement thickness actually used to obtain the new displacement surface ordinates are updated from one iteration to the next using under-relaxation, i.e.,

$$\delta^*_{new} = \delta^*_{old} + w(\delta^* - \delta^*_{old})$$

where w is a relaxation parameter and δ^* is the displacement thickness calculated using the latest pressure distribution.

To obtain the boundary layer solution from the airfoil pressure distribution, the flow is assumed to be initially laminar at the leading edge stagnation point. In this region, a compressible Thwaites method, which is an efficient one parameter intregral method, is utilized to obtain the boundary layer properties; and, once it has been determined that the flow has transitioned from laminar to turbulent, the viscous layer is solved using the Nash-Macdonald method with smoothing. The location of the transition point is determined from a Granville type correlation based upon the difference between the local momentum thickness Reynold's number and the value at the laminar instability point combined with the pressure gradient history. Sometimes, at high angles of attack, laminar separation is predicted upstream of this transition point on the upper surface.

If this situation occurs, the local momentum thickness Reynold's number is compared to an empirical correlation in order to determine if the resultant laminar bubble is long or short. Normally, the bubble is of the short type. If, however, it is long, the present model is not applicable and the subsequent calculations will probably be in error. In either case, transition to turbulent flow is assumed at the next grid point, and the calculation is continued.

As stated, the Nash-Macdonald method together with certain smoothing operations is used to compute boundary layer properties in the turbulent flow region. In order to determine the boundary layer displacement thickness, the momentum integral equation must be satisfied for the momentum thickness . This equation is

$$\frac{d\theta}{ds} + (H + 2 - m^2)\frac{\theta}{q}\frac{dq}{ds} = \tau_w$$

and it is solved in conjunction with the formulas of Nash and Macdonald for skin friction, τ_w , and the shape factor, $H = \delta^*/\theta$. This equation is numerically integrated at each grid point along the airfoil surface, and the resulting set of displacement thickness are then smoothed. At the trailing edge, an extrapolation procedure is used to obtain the trailing edge displacement thickness. The smoothing used in this procedure reduces the rapid variations which sometimes occur in regions with large pressure gradients, such as near shock waves. It should be noted that the Nash-Macdonald method with smoothing and extrapolation yields an overall and trailing edge behavior that agrees with the observed effect of the boundary layer on pressure distribution and lift.

The procedure for inclusion of viscous interaction in the embedded grid case is similar to that used in the main grid where input to the boundary layer calculation routine consists of the pressure distribution and airfoil coordinates. Since the embedded grid consists only of points near the leading edge of the airfoil, the embedded grid solution must be interfaced to the main grid solution for input to the boundary layer calculation routine.

Each time the displacement surface is updated, the pressure distribution for the embedded grid region is calculated and used in that region; and, the pressure distribution from the last main grid solution is used for the remainder of the airfoil. This new pressure distribution is then used to calculate the airfoil boundary layer characteristics; and, the boundary layer displacement surface is updated.

The original reason for considering a coupled solution of the main and embedded grids was to correctly model the effects of very weak shock induced viscous effects. These effects occur with the airfoil at a fairly high angle of attack in a medium (0.3-0.5) Mach number flow. At these conditions, a small shock wave may be located very near the airfoil leading edge. Although this shock wave would be too small to detect using the main grid, the embedded grid should be able to capture it. This resolution should be very significant since even a small shock wave can have major effects on the subsequent development of the airfoil boundary layer. A coupled main-embedded grid solution is necessary, therefore, to determine the effects of such a shock wave over the entire airfoil surface.

In the cases previously reported [1], the solution of the embedded grid always occurred after the main grid solution had been completed. However, to make a coupled solution possible, some method had to be developed in which the embedded grid influenced the main grid. Several possible approaches were investigated, but these did not yield any significant improvements when compared to the main grid only solution. The present coupled method, however, allows small changes in the viscous boundary layer to affect the main grid solution, which is physically realistic.

In the coupled solution scheme, the main grid solution is started in the usual fashion. However, at the time the viscous boundary layer update is usually performed, an embedded grid solution is obtained instead.

This procedure is followed by the viscous boundary layer update routine modified to include the embedded grid solution. After the boundary layer characteristics of the composite airfoil solution have been determined, a spline curve fit is used to update the displacement surface ordinates. The perturbation potentials and the other inviscid flowfield parameters from the previous main grid solution are not altered. The main grid solution routine is then continued with the updated displacement surface. A flow chart of this procedure is shown in Figure 2.

Through numerical studies conducted as part of this research, an iteration procedure has been determined which rapidly and accurately converged to the final flowfield solution. First, two coarse Cartesian grids are solved completely inviscidly. These grids are typically 13x7 and 25x13, although they can be varied by the user. These two Cartesian grids provide an initial solution to the finer Cartesian grids. On the third (typically 49x25) and remaining main grids, fifty inviscid iterations are completed initially, at which point an embedded grid solution is obtained. However, it is limited to one hundred iterations. Then, the embedded grid solution and the latest main grid solution are used together to determine the boundary layer properties. As noted previously, a spline curve fit updates the displacement surface ordinates. Subsequently, the main grid solution scheme continues for twenty more iterations, followed by another embedded grid solution and a displacement surface update.

To increase the rate of convergence during initial boundary layer calculations, the relaxation parameter, w, is nominally set initially to 0.50. When the change in δ^* at the trailing edge from one viscous update to the next drops below ten percent, w is reduced to 0.25.

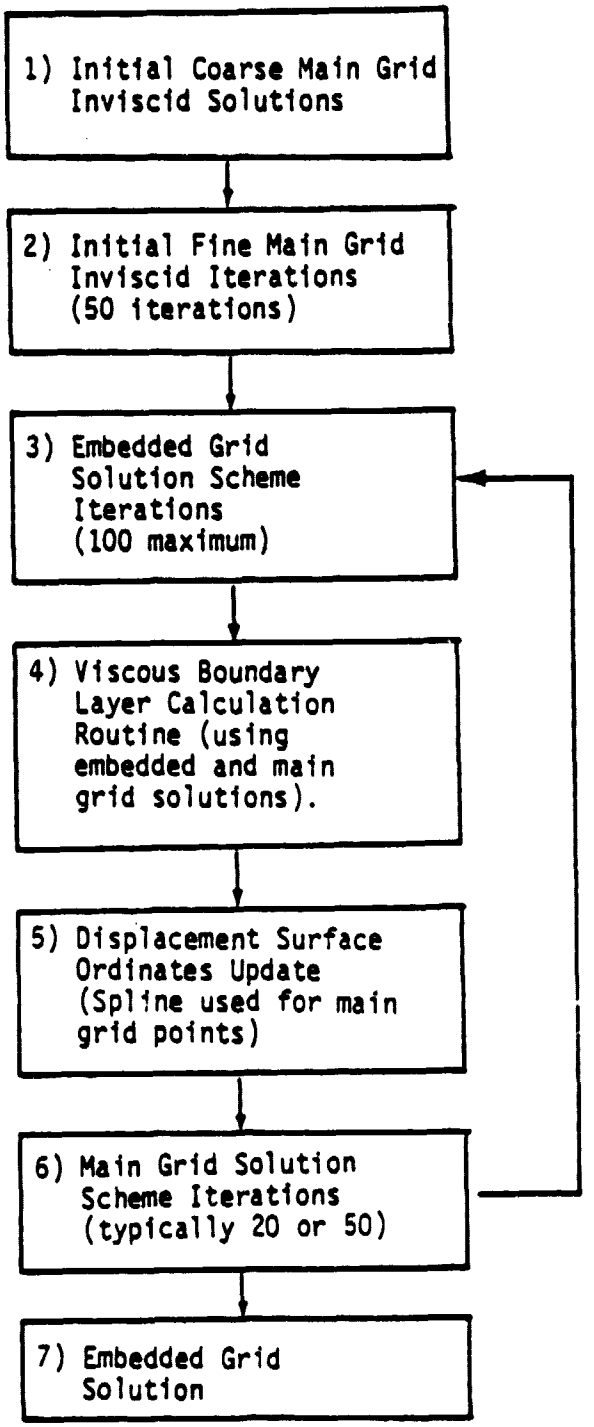

Figure 2 - Coupled Main-Embedded Grid Solution Procedure

Frequently, the δ^* at the trailing edge converges very rapidly. In order to take advantage of this fact and to reduce computing time, the frequency of viscous updating is reduced to every fifty iterations once the change in δ^* at the trailing edge is less than 0.0001.

In order to further promote a converged solution, a certain number of iterations are set aside at the end of the procedure in which no displacement surface updates are computed. For the finest main grid selected, no updates are calculated after eighty percent of the maximum number of iterations has occurred for that grid. For the previous main grid no updates are made after 350 iterations.

Once the main grid solution has been reached, a final inviscid embedded grid solution is conducted so that the calculated lift and drag coefficients have the greatest amount of accuracy available.

Several test runs have been conducted to verify the coupled main-embedded grid viscous solution method. The test cases chosen were for a completely subcritical flowfield, a slightly supercritical flowfield, and a highly supercritical flowfield. In each case, in order to minimize computer costs, only a 49x25 main grid with 25 points on each surface of the airfoil was used.

The completely subcritical test case consisted of a NACA 0012 airfoil at a zero degree angle of attack and a Mach number of 0.10. The embedded grid used 79 points on the airfoil and extended rearward to x/c = -0.213. The pressure distribution for this case is shown in Figure 3 along with the pressure distribution for a similar case using the main grid only for solution. Notice that the C_p's were slightly lower for the coupled solution than for the main grid alone solution. The drag coefficient due to friction (C_{df}) of the two solutions were also in good agreement. The C_{df} of the coupled solution was 0.0043 while that of the main grid only solution was 0.0049.

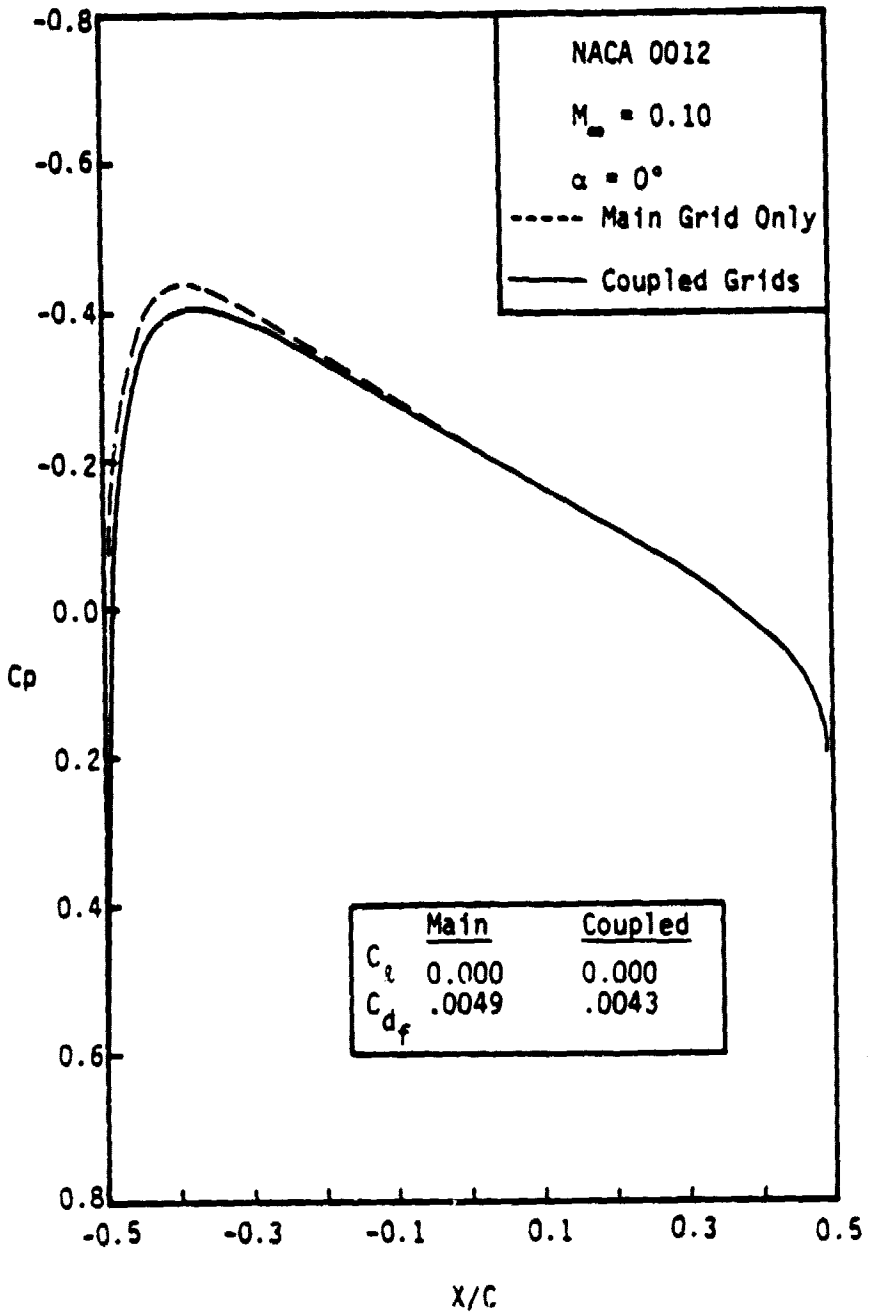

Figure 3 - Completely Subcritical Viscous Coupled Solution Comparison

The trailing edge displacement thickness, δ^* of the main grid only solution converged to 0.0036, while the coupled solution case trailing edge δ^* converged to 0.0029.

The slightly supercritical test case consisted of a NACA 0012 airfoil at an angle of attack of one degree and a Mach number of 0.72. The embedded grid used 85 points on the airfoil surface and extended rearward to x/c=0.18070. The pressure distribution of this case is shown in Figure 4 again compared to a similar result using only a main grid solution. Notice that the C_p's obtained from the main grid only scheme were higher than those resulting from the coupled solution procedure. As in the preceding case, the C_{df} of the coupled solution was of the same order of magnitude but slightly lower than the C_{df} of the main grid only solution. In this case, the C_{df} of the coupled solution was 0.0046 while the C_{df} of the main grid only solution was 0.0048. The δ^* at the trailing edge of the two solutions also converged to similar results, with the coupled solution δ^* being slightly higher at 0.0064. The δ^* at the trailing edge for the main grid only solution was 0.0060. In both cases, a short separation bubble was formed at the upper surface transition location. The location at which this ocurred was in very good agreement between the two solutions. The main grid only solution predicted the bubble and transition at x/c = -0.28287, while the coupled solution method predicted this bubble would occur at -0.28466.

The highly supercritical test case consisted of a NACA 0012 airfoil at a Mach number of 0.80 and an angle of attack of zero degrees. The embedded grid used 79 points on the airfoil and extended rearward to x/c = -0.213. The pressure distribution of this case is shown in Figure 5 along with a similar result using only a main grid solution.

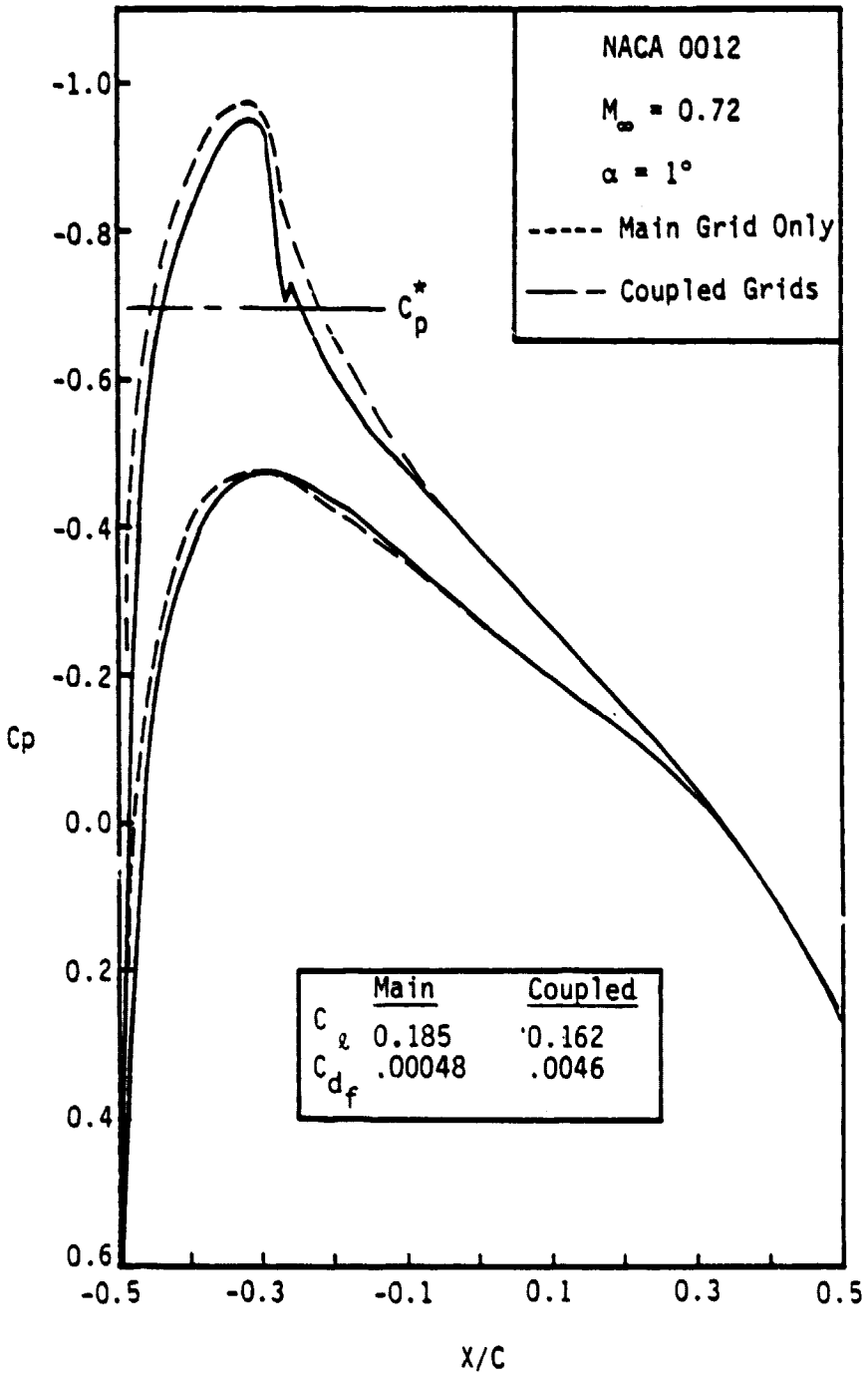

Figure 4 - Slightly Supercritical Viscous Coupled Solution Comparison

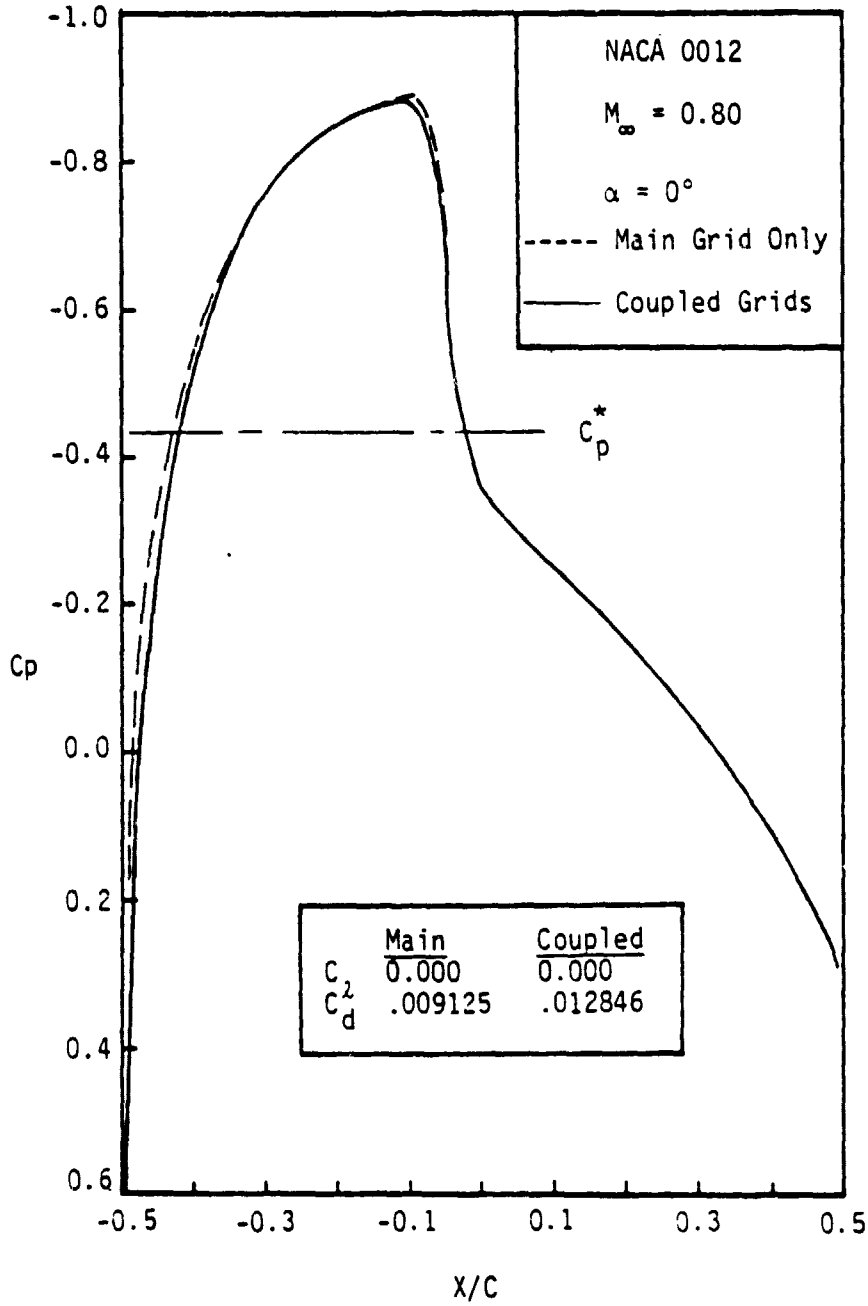

Figure 5 - Highly Supercritical Viscous Coupled Solution Comparison

Notice that the C_p's obtained from the main grid only scheme were almost identical to those resulting from the coupled solution procedure. Again, the C_{df} of the coupled solution was of the same order of magnitude but slightly lower than the C_{df} of the main grid only solution. In this case, the C_{df} of the coupled solution was 0.0037 while the C_{df} of the main grid only solution was also 0.0037. However, the slight changes in the C_p distribution near the leading edge greatly improved the total drag. In the main grid only case, the total C_d was only 0.0091 but with the embedded grid it was more reasonable 0.0128. The δ^* at the trailing edge for the two solutions again converged to similar values, with the coupled solution being 0.0045 while the main grid only solution converged to a δ^* of 0.0046. The location of the transition from laminar to turbulent point was again in excellent agreement between the two solutions. The main grid only solution and the coupled solution both predicted transition at x/c = 0.09803. This agreement verifies that the introduction of the embedded grid viscous approach and its accompanying fine resolution enhances without degrading the accuracy of the boundary layer solution.

Based upon these results, the following conclusions can be stated:

1) A body-fitted grid embedment technique applicable to inviscid transonic airfoil flowfield analysis has been developed and verified through a series of test cases.
2) Test cases used to verify the inviscid transonic airfoil flowfield grid embedment analysis technique show that the accuracy of the solution has been increased by grid embedding. This enhancement of the solution has been especially true when small supercritical zones occur which cannot be adequately described using the main grid only.

3) Viscous interaction has been applied to the body-fitted grid embedment analysis technique using the Thwaite's and Nash-Macdonald techniques. To obtain accurate results, however, it has been determined that the main and embedded viscous interaction solutions must be obtained by some type of coupled technique.

4) A technique for solving the viscous, transonic airfoil flowfield using a coupled main and embedded grid has been developed and verified through a series of test cases.

5) The test cases used to verify the coupled main-embedded grid solution technique show that the leading edge resolution is significantly increased without degrading the boundary layer solution.

6) Results show that the embedded grid region can contain the entire supercritical zone or only a portion of it and still produce accurate results. It is noted, however, that placement of the main-embedded grid interface at the shock wave tends to degrade the solution.

During the next reporting period, an attempt will be made to put existing embedded grid code into a more user orientated form. A rough draft of a user's manual has already been written, and it is planned to finalize this manual and issue it either as a NASA document or as a Texas Engineering Experiment Station report.

IV. Massive Separation Studies

In the last progress report[1], several results obtained with the SKANFP full potential program were presented. This program is designed to handle massive separated flow and high lift and uses the simplified Kuhn-Nielsen turbulent boundary layer method as modified by Barnwell[2].

As previously noted, the resultant C_p values exhibited an undesirable and unrealistic "bump" in the vicinity of the separation point due to a mismatch between the unseparated and separated pressure distributions.

During this reporting period, several techniques have been studied in an attempt to eliminate this feature. After extensive investigation, this problem has been traced to the flowfield solution at the point just before separation, primarily in the value of the displacement surface slope just before the separation point. This value was previously determined by smoothing the displacement thickness, adding the smoothed values to the original ordinates, and spline fitting the resultant surface. The spline fit was then used to determine the derivatives of the displacement surface. Unfortunately, the δ^*'s used in this procedure included values in the separation zone predicted by the boundary layer calculations which may not agree with the shape determined by the inverse procedure in the separated zone.

It was thought that perhaps the smoothing process was contributing to the problem since it would permit points in the separation zone to influence upstream points. Thus, a run with no smoothing on the upper surface displacement thickness was tried. Unfortunately, the results were oscillatory and unstable, indicating that smoothing was important to the overall process.

Subsequent investigation indicated that an important quality affecting the results at the point before separation is the upper surface displacement slope. This value is "normally" determined by the spline fit routine. However, an alternative approach would be to compute it from the values of the displacement surface ordinate, and the U and V velocity components at that location. This approach has been tried, and resultant slopes are compared to the original values on Figure 6. As can be seen, the original results (SKAN64) exhibit significant change just before separation; while the new data (SKAN66) is much smoother.

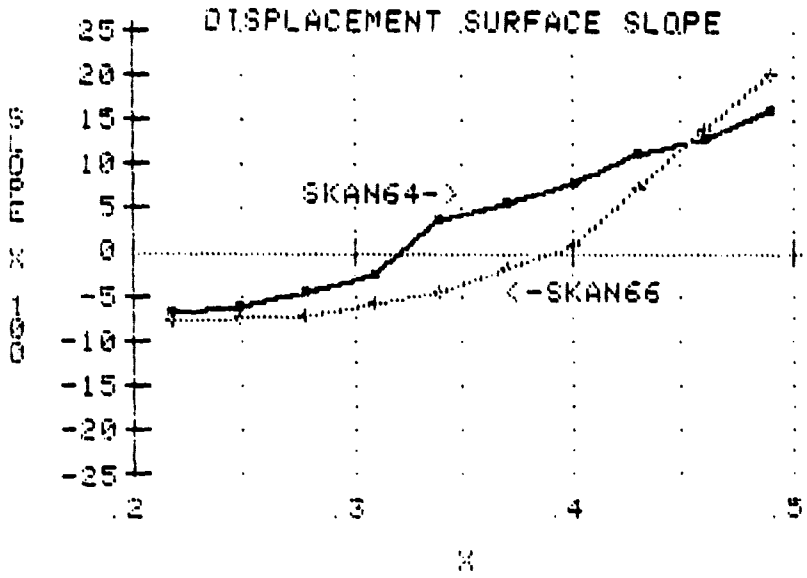

Figure 6 -- Comparison of Upper Surface Slopes

This new approach looks promising; and it, among others, will be investigated in more detail in the future.

While the present results appear reasonable, significant problems still exist when they are compared to experimental data. Figure 7 compares the SKAN66 pressure distribution with test data obtained in the Langley LTPT wind tunnel. It appears that the present SKANFP method is predicting separation too far downstream. This possiblity will be investigated, and methods of correcting it will be developed.

V. Publications

During the present reporting period, the following publication was issued:

Reed, Christopher L., "Grid Embedment as Applied to Viscous Transonic Airfoil Flowfield Analysis", M. Sc. Thesis, Texas A&M University, December 1981.

Vl. References

1. Carlson, L.A., "Inverse Transonic Airfoil Design Methods, etc. Progress Report," TAMRF Report No. 3224-81-02, August 1981.

2. Barnwell, R.N., "A Potential-Flow Boundary-Layer Method for Calculating Subsonic and Transonic Airfoil Flow with Trailing-Edge Separation," NASA TM-81850, June 1981.

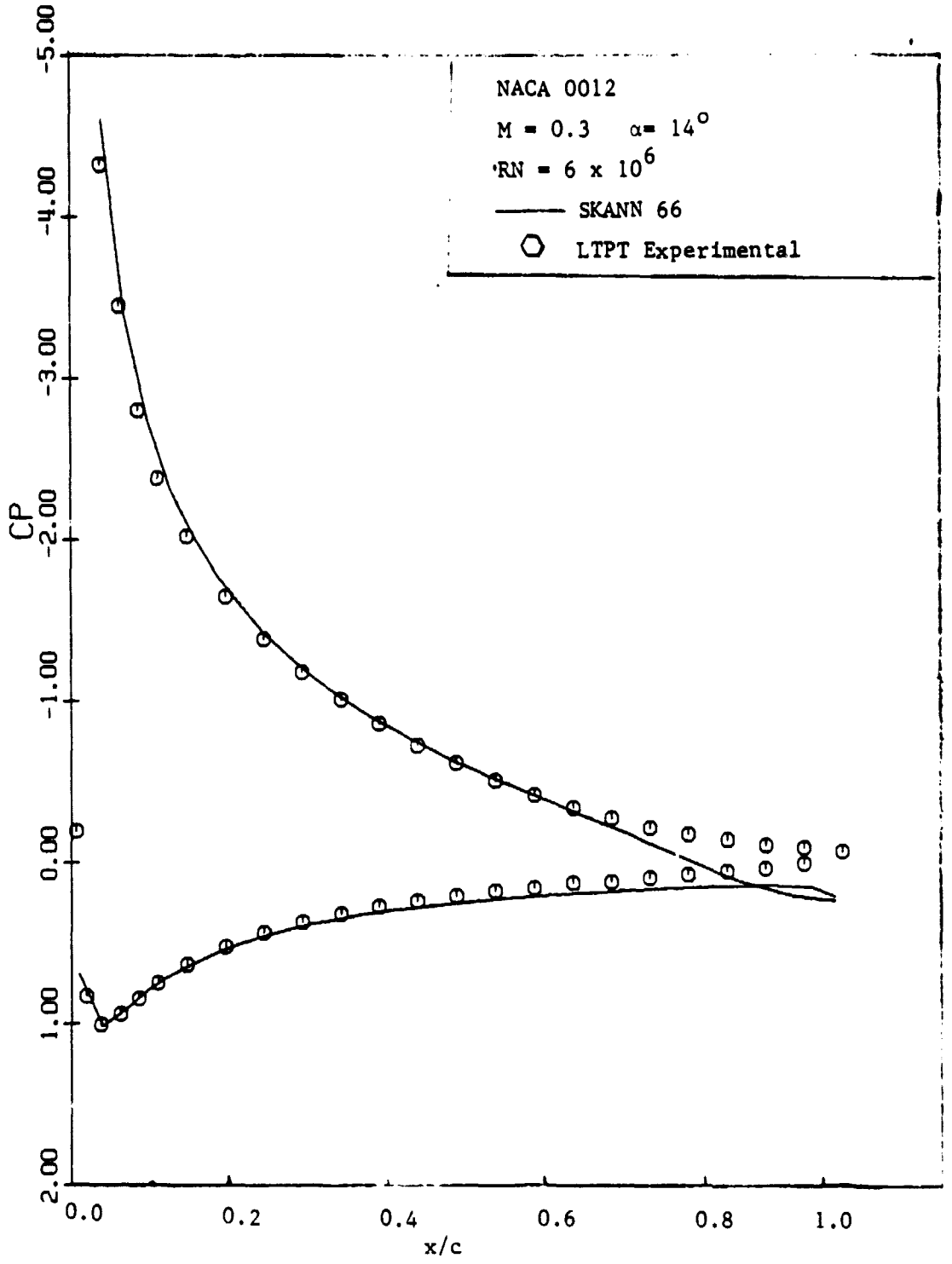

Figure 7 -- Comparison of SKANN 66 with Experiment